NASA TECHNICAL NOTE

NASA TN D-7839

NASA TN D-7839



# ANALYSIS OF THE DYNAMIC RESPONSE OF A SUPERSONIC INLET TO FLOW-FIELD PERTURBATIONS UPSTREAM OF THE NORMAL SHOCK

*Gary L. Cole and Ross G. Willoh*

*Lewis Research Center*
*Cleveland, Ohio 44135*

NATIONAL AERONAUTICS AND SPACE ADMINISTRATION • WASHINGTON, D. C. • JANUARY 1975

| 1. Report No. | 2. Government Accession No. | 3. Recipient's Catalog No. |
|---|---|---|
| NASA TN D-7839 | | |

| 4. Title and Subtitle | 5. Report Date |
|---|---|
| ANALYSIS OF THE DYNAMIC RESPONSE OF A SUPERSONIC INLET TO FLOW-FIELD PERTURBATIONS UPSTREAM OF THE NORMAL SHOCK | January 1975 |
| | 6. Performing Organization Code |

| 7. Author(s) | 8. Performing Organization Report No. |
|---|---|
| Gary L. Cole and Ross G. Willoh | E-7969 |
| | 10. Work Unit No. 501-24 |

| 9. Performing Organization Name and Address | 11. Contract or Grant No. |
|---|---|
| Lewis Research Center<br>National Aeronautics and Space Administration<br>Cleveland, Ohio 44135 | |

| 12. Sponsoring Agency Name and Address | 13. Type of Report and Period Covered |
|---|---|
| National Aeronautics and Space Administration<br>Washington, D.C. 20546 | Technical Note |
| | 14. Sponsoring Agency Code |

15. Supplementary Notes

16. Abstract

A linearized mathematical analysis is presented for determining the response of normal shock position and subsonic duct pressures to flow-field perturbations upstream of the normal shock in mixed-compression supersonic inlets. The inlet duct cross-sectional area variation is approximated by constant-area sections; this approximation results in one-dimensional wave equations. A movable normal shock separates the supersonic and subsonic flow regions, and a choked exit is assumed for the inlet exit condition. The analysis leads to a closed-form matrix solution for the shock position and pressure transfer functions. Analytical frequency response results are compared with experimental data and a method of characteristics solution.

| 17. Key Words (Suggested by Author(s)) | | 18. Distribution Statement |
|---|---|---|
| Analysis | Air intakes | Unclassified - unlimited |
| Supersonic inlets | Inlet dynamics | STAR category 28 |
| Mixed-compression inlets | Frequency response | |

| 19. Security Classif. (of this report) | 20. Security Classif. (of this page) | 21. No. of Pages | 22. Price* |
|---|---|---|---|
| Unclassified | Unclassified | 37 | $3.25 |

* For sale by the National Technical Information Service, Springfield, Virginia 22151

# ANALYSIS OF THE DYNAMIC RESPONSE OF A SUPERSONIC INLET TO FLOW-FIELD PERTURBATIONS UPSTREAM OF THE NORMAL SHOCK

by Gary L. Cole and Ross G. Willoh

Lewis Research Center

## SUMMARY

A linearized mathematical analysis of supersonic inlet dynamics is presented. Attention is concentrated on determining the response of normal shock position and subsonic duct pressures to flow-field perturbations upstream of the normal shock in mixed-compression inlets. The analysis is based on a previous NASA report which dealt primarily with perturbations downstream of the normal shock.

The inlet duct cross-sectional area variation is approximated by constant area sections. This approximation, in combination with a linearized analysis, results in one-dimensional wave equations for each duct section. The supersonic and subsonic flow regions are separated by a movable normal shock. A choked exit is assumed for the inlet exit condition. The analysis leads to a closed-form matrix solution for the shock position and pressure transfer functions.

The analysis was compared on a frequency response basis with a method-of-characteristics solution. The agreement in both amplitude ratio and phase was excellent.

Analytical frequency response results were also compared with experimental data. The phase angle results were generally in good agreement. Amplitude ratio response curves, although not in as good agreement as phase data, showed generally good agreement in shape. Some shifts in low-frequency gain were found, however.

## INTRODUCTION

Propulsion system performance of supersonic aircraft depends greatly on the type of inlet system being used. Mixed-compression inlets are best for achieving high propulsion system performance in aircraft that fly at Mach numbers in excess of about 2.0. Because of the nature of mixed-compression inlet design, a normal shock wave usually exists within the inlet during supersonic operation. For best inlet performance the normal shock must be positioned near the throat where the shock is susceptible to being

displaced by disturbances arising from such things as atmospheric perturbations, aircraft maneuvers, and changes in engine operation. A downstream displacement of the shock results in a loss of inlet performance. If the shock is displaced in the upstream direction, it is in danger of being expelled from the inlet. This is referred to as inlet unstart. Inlet unstart may result in undesirable consequences such as compressor stall, combustor flameout, reduced propulsion system thrust and increased vehicle drag. To counteract such possibilities, mixed-compression inlets are provided with variable geometry features that can be automatically controlled to keep the shock at the desired position. The design of these shock-position control systems requires knowledge of the shock-position dynamic response to perturbations in the inlet. The purpose of this report is to develop an approximate mathematical analysis for predicting the dynamic response of shock position and pressures, in mixed-compression inlets to perturbations upstream of the normal shock.

In the past a great deal of attention has been given to controlling shock position against airflow perturbations originating downstream of the normal shock (refs. 1 to 6). Normal shock motion due to perturbations downstream of the shock has been examined analytically (e.g., refs. 7 and 8). Reference 9 presents a mathematical analysis that is valid for obtaining shock responses to perturbations downstream or just upstream of the normal shock. However, the upstream terms were dropped and consideration was restricted to the downstream case. Reference 10 does deal with upstream perturbations and presents an analysis that includes both storage-volume and Helmholtz-mass effects. Reference 11 presents transfer functions for shock position to upstream perturbations. The transfer functions vary in complexity from first to fourth order, and results are compared with a method-of-characteristics solution. The fourth-order model is a linearized version of the analysis in reference 10.

In this report a mathematical analysis is presented that combines a set of linearized equations across the normal shock with an exact solution of the linearized one-dimensional wave equation. This analysis is based on the analysis of reference 9. Use of this technique avoids the complexity of the method of characteristics while still predicting the resonances of a distributed parameter system. However, flow-field discontinuities due to oblique shock waves in the supersonic duct are neglected. The analysis presented is more exact than conventional lumped-parameter techniques and for frequency response results no more complicated in application. If transient responses are desired the equations are especially suitable for analog simulation. The analysis is followed by a matrix solution that provides a simple means for obtaining frequency responses on a digital computer. Finally, analytical frequency responses are compared with results from a method-of-characteristics solution found in reference 11 and with experimental data obtained during a wind tunnel program. Dr. Frank Barry of the Hamilton Standard Company supplied us with information regarding the method-of-characteristics analysis in addition to that in reference 11.

## MATHEMATICAL ANALYSIS

The analysis presented in this report is an extension of the analysis in reference 9. In this report prime consideration is given to perturbations upstream of the normal shock. The symbols used in this report (and defined in the appendix) are consistent with those of reference 9.

A schematic of an ideal mixed-compression inlet is shown in figure 1. In reference 9 a set of linearized equations relating normal shock position to adjacent parameters was developed using total pressure, flow, and entropy as state variables. In addition, a linearization of the compressible flow equations written in terms of the state variables was used to develop a set of wave equations for the subsonic duct. In the analysis of this report the same wave equations are applied to both the subsonic and supersonic flow regions. The normal shock position equations are used to couple the subsonic and supersonic duct sections and a choked exit is used as the downstream boundary condition for the subsonic duct.

### Shock-Position Dynamics

Equations relating normal shock position and velocity to adjacent upstream and downstream variables (total pressure, airflow, and entropy) were obtained using the following assumptions: perfect-gas relations, a constant specific-heat ratio of 1.4, and negligible change in duct area across the normal shock. The normal shock equations are (ref. 9, eqs. (1) to (3)):

$$\frac{\Delta P_{T,2}}{\bar{P}_{T,2}} = \frac{6}{7\bar{M}_1^2 - 1}\frac{\Delta P_{T,1}}{\bar{P}_{T,1}} - \frac{7\left(\bar{M}_1^2 - 1\right)}{7\bar{M}_1^2 - 1} R_c \frac{A'}{A}\left(\frac{\Delta X_s}{R_c}\right)$$

$$- \frac{7\left(\bar{M}_1^2 - 1\right)}{7\bar{M}_1^2 - 1} R_c \frac{5\left(1 + 0.2\,\bar{M}_1^2\right)^{1/2}}{6\bar{a}_T \bar{M}_1}\frac{d}{dt}\left(\frac{\Delta X_s}{R_c}\right) + \frac{7\left(\bar{M}_1^2 - 1\right)}{7\bar{M}_1^2 - 1}\left(\frac{\Delta \dot{W}_1}{\bar{W}_1} + \frac{\Delta a_{T,1}}{\bar{a}_T}\right) \quad (1)$$

$$\frac{\Delta \dot{W}_2}{\bar{W}_1} = \frac{\Delta \dot{W}_1}{\bar{W}_1} + \frac{1}{\bar{a}_T \bar{M}_1}\frac{\bar{M}_1^2 - 1}{\left(1 + 0.2\,\bar{M}_1^2\right)^{1/2}} R_c \frac{d}{dt}\left(\frac{\Delta X_s}{R_c}\right) \quad (2)$$

$$\frac{\Delta S_2}{R} = \frac{\Delta S_1}{R} - \frac{7\left(\overline{M}_1^2 - 1\right)}{7\overline{M}_1^2 - 1}\left(\frac{\Delta \dot{W}_1}{\overline{\dot{W}}_1} + \frac{\Delta a_{T,1}}{\bar{a}_T} - \frac{\Delta P_{T,1}}{\overline{P}_{T,1}}\right) + \frac{7\left(\overline{M}_1^2 - 1\right)}{7\overline{M}_1^2 - 1} R_c \frac{A'}{A}\left(\frac{\Delta X_s}{R_c}\right)$$

$$- \frac{7\left(\overline{M}_1^2 - 1\right)}{7\overline{M}_1^2 - 1} R_c \frac{\overline{M}_1^2 - 1}{\bar{a}_T \overline{M}_1 \left(1 + 0.2\,\overline{M}_1^2\right)^{1/2}} \frac{d}{dt}\left(\frac{\Delta X_s}{R_c}\right) \qquad (3)$$

where the subscripts 1 and 2 designate fixed stations just upstream and just downstream of the shock (fig. 1), respectively. There are two differences between equations (1) to (3) herein and those of reference 9. One is that shock position is normalized by the radius of the inlet cowl lip $R_c$ instead of by the length of the subsonic duct ($L_T$ in ref. 9). ($R_c$ is a more convenient normalizing parameter because it is a constant, whereas $L_T$ depends on the shock operating point.) The other difference is that equations (1) to (3) herein have the quantity $\overline{\dot{W}}_1$; in reference 9 the subscript 1 was omitted. In this analysis the airflow rates will be normalized by the steady-state airflow at the most upstream station, designated as $\overline{\dot{W}}_\infty$. To obtain the correct normalized airflow rates the $\Delta\dot{W}_1/\overline{\dot{W}}_1$ terms in equations (1) and (3) must be multiplied by the ratio $\overline{\dot{W}}_\infty/\overline{\dot{W}}_\infty$, and equation (2) must be multiplied by $\overline{\dot{W}}_1/\overline{\dot{W}}_\infty$.

Equations (1) and (3) contain the variable $\Delta a_{T,1}/\bar{a}_T$, which is not independent of $(\Delta S_1/R)$ and $(\Delta P_{T,1}/\overline{P}_{T,1})$. The $\Delta a_{T,1}/\bar{a}_T$ terms can be eliminated by means of the following equation (ref. 11):

$$\frac{\Delta a_T}{\bar{a}_T} = \frac{1}{7}\left(\frac{\Delta P_T}{\overline{P}_T} + \frac{\Delta S}{R}\right) \qquad (4)$$

Using equation (4) to eliminate $\Delta a_{T,1}/\bar{a}_T$ terms and including the multiplications involving $\overline{\dot{W}}_1$ and $\overline{\dot{W}}_\infty$, equations (1) to (3) become

$$\frac{\Delta P_{T,2}}{\overline{P}_{T,2}} = \frac{\overline{M}_1^2 + 5}{7\overline{M}_1^2 - 1}\left(\frac{\Delta P_{T,1}}{\overline{P}_{T,1}}\right) + \frac{\overline{M}_1^2 - 1}{7\overline{M}_1^2 - 1}\left(\frac{\Delta S_1}{R}\right) + \frac{7\left(\overline{M}_1^2 - 1\right)}{7\overline{M}_1^2 - 1}\frac{\overline{\dot{W}}_\infty}{\overline{\dot{W}}_1}\left(\frac{\Delta \dot{W}_1}{\overline{\dot{W}}_\infty}\right)$$

$$- \frac{7\left(\overline{M}_1^2 - 1\right)}{7\overline{M}_1^2 - 1} R_c \left[\frac{A'}{A}\left(\frac{\Delta X_s}{R_c}\right) + \frac{5\left(1 + 0.2\,\overline{M}_1^2\right)^{1/2}}{6\bar{a}_T \overline{M}_1}\frac{d}{dt}\left(\frac{\Delta X_s}{R_c}\right)\right] \qquad (5)$$

$$\frac{\Delta \dot{W}_2}{\overline{\dot{W}}_\infty} = \frac{\Delta \dot{W}_1}{\overline{\dot{W}}_\infty} + \frac{\dot{W}_1}{\bar{a}_T \overline{M}_1 \overline{\dot{W}}_\infty} \frac{\overline{M}_1^2 - 1}{\left(1 + 0.2\,\overline{M}_1^2\right)^{1/2}} R_c \frac{d}{dt}\left(\frac{\Delta X_s}{R_c}\right) \qquad (6)$$

$$\frac{\Delta S_2}{R} = \frac{6\overline{M}_1^2}{7\overline{M}_1^2 - 1}\left(\frac{\Delta S_1}{R}\right) - \frac{7\left(\overline{M}_1^2 - 1\right)}{7\overline{M}_1^2 - 1}\frac{\overline{\dot{W}}_\infty}{\overline{\dot{W}}_1}\left(\frac{\Delta \dot{W}_1}{\overline{\dot{W}}_\infty}\right) + \frac{6\left(\overline{M}_1^2 - 1\right)}{7\overline{M}_1^2 - 1}\left(\frac{\Delta P_{T,1}}{\overline{P}_{T,1}}\right)$$

$$+ \frac{7\left(\overline{M}_1^2 - 1\right)}{7\overline{M}_1^2 - 1} R_c \left[\frac{A'}{A}\frac{\Delta X_s}{R_c} - \frac{\overline{M}_1^2 - 1}{\bar{a}_T \overline{M}_1 \left(1 + 0.2\,\overline{M}_1^2\right)^{1/2}}\frac{d}{dt}\left(\frac{\Delta X_s}{R_c}\right)\right] \tag{7}$$

Equations (5) to (7) can be written in terms of the Laplace transform as

$$\tilde{P}_2 = C_4\tilde{P}_1 + \frac{C_1}{C_r}\tilde{\dot{W}}_1 + \frac{C_1}{7}\tilde{S}_1 - C_1\left(R_c\frac{A'}{A} + C_2 s\right)\tilde{X}_s \tag{8}$$

$$\tilde{\dot{W}}_2 = \tilde{\dot{W}}_1 + C_r C_3 s\,\tilde{X}_s \tag{9}$$

$$\tilde{S}_2 = \frac{6}{7}C_1\tilde{P}_1 - \frac{C_1}{C_r}\tilde{\dot{W}}_1 + C_5\tilde{S}_1 + C_1\left(R_c\frac{A'}{A} - C_3 s\right)\tilde{X}_s \tag{10}$$

where

$$C_1 = \frac{7\left(\overline{M}_1^2 - 1\right)}{7\overline{M}_1^2 - 1}$$

$$C_2 = \frac{5\left(1 + 0.2\,\overline{M}_1^2\right)^{1/2}}{6\bar{a}_T\overline{M}_1} R_c$$

$$C_3 = \frac{1}{\bar{a}_T\overline{M}_1}\frac{\overline{M}_1^2 - 1}{\left(1 + 0.2\,\overline{M}_1^2\right)^{1/2}} R_c$$

$$C_4 = \frac{\overline{M}_1^2 + 5}{7\overline{M}_1^2 - 1}$$

$$C_5 = \frac{6\overline{M}_1^2}{7\overline{M}_1^2 - 1}$$

$$C_r = \frac{\overline{\dot{W}_1}}{\overline{\dot{W}_\infty}}$$

$$\tilde{P} = \frac{\Delta P_T(s)}{\overline{P}_T}$$

$$\tilde{\dot{W}} = \frac{\Delta \dot{W}(s)}{\overline{\dot{W}}}$$

$$\tilde{S} = \frac{\Delta S(s)}{R}$$

and

$$\tilde{X}_s = \frac{\Delta X_s}{R_c}(s)$$

Supersonic inlets often have provisions for bleed flow in the vicinity of the normal shock operating point to increase inlet stability. The analysis of reference 9 did not include the effects of stability bleed in the normal shock equations (8) to (10). If the effects of small perturbations in pressure are neglected, such bleed flows are proportional to shock position. Reference 12 shows that for such a bleed equation (9) becomes

$$\tilde{\dot{W}}_2 = \tilde{\dot{W}}_1 + \left(C_B + C_r C_3 s\right) \tilde{X}_s \tag{11}$$

where

$$C_B = \frac{\left(\Delta \dot{W}_B / \overline{\dot{W}}_\infty\right)}{\left(\Delta X_s / R_c\right)}$$

## Duct Wave Equations

The wave equations were derived in reference 9 as the solution for the subsonic duct. The following assumptions were made: perfect gas relations, a constant specific-heat ratio of 1.4, an inviscid nonheat-conducting fluid, and negligible change in duct area that might result from boundary-layer effects or changes in inlet geometry.

These assumptions are not restrictive to subsonic flow. However, discontinuities in entropy and total pressure due to oblique shock waves in the supersonic portion of the duct are neglected. The linearized one-dimensional wave equations are (eqs. (96)

to (98), ref. 9):

$$\left[\frac{\partial}{\partial t} + (v + a)\frac{\partial}{\partial x}\right]\left(\frac{\Delta P_T}{\overline{P}_T} + \alpha\frac{\Delta \dot{W}}{\overline{\dot{W}}} + \beta\frac{\Delta S}{R}\right) = 0 \tag{12}$$

$$\left[\frac{\partial}{\partial t} + (v - a)\frac{\partial}{\partial x}\right]\left(\frac{\Delta P_T}{\overline{P}_T} - \alpha\frac{\Delta \dot{W}}{\overline{\dot{W}}} - \gamma\frac{\Delta S}{R}\right) = 0 \tag{13}$$

$$\left(\frac{\partial}{\partial t} + v\frac{\partial}{\partial x}\right)\frac{\Delta S}{R} = 0 \tag{14}$$

where

$$\alpha = \frac{7M_{av}}{M_{av}^2 + 5}$$

$$\beta = \frac{M_{av}\left(M_{av} + 2\right)}{M_{av}^2 + 5}$$

$$\gamma = \frac{M_{av}\left(2 - M_{av}\right)}{M_{av}^2 + 5}$$

The solutions of equations (12) to (14) may be used to relate properties between two stations, n and n + 1, in a duct of length L. In Laplace transform notation the results are

$$\tilde{P}_{n+1} + \alpha\tilde{\dot{W}}_{n+1} + \beta\tilde{S}_{n+1} = e^{-\sigma s}\left(\tilde{P}_n + \alpha\tilde{\dot{W}}_n + \beta\tilde{S}_n\right) \tag{15}$$

$$\tilde{P}_{n+1} - \alpha\tilde{\dot{W}}_{n+1} - \gamma\tilde{S}_{n+1} = e^{\tau s}\left(\tilde{P}_n - \alpha\tilde{\dot{W}}_n - \gamma\tilde{S}_n\right) \tag{16}$$

$$\tilde{S}_{n+1} = e^{-\theta s}\left(\tilde{S}_n\right) \tag{17}$$

where

$$\sigma = \frac{L}{(v + a)} = \frac{L}{a(M + 1)}$$

$$\tau = \frac{L}{a - v} = \frac{L}{a(1 - M)}$$

$$\theta = \frac{L}{v} = \frac{L}{aM}$$

Equations (15) and (17) represent the propagation of waves traveling downstream. Equation (16) also represents the propagation of a wave, but the direction depends on the value of M. In supersonic flow (M > 1) the wave travels downstream and in subsonic flow (M < 1) it travels upstream.

Equations (15) to (17) are valid only for a constant-area duct. Variations in inlet duct area are approximated by dividing the inlet into a series of constant-area ducts. The Mach number in a duct section is averaged by summing one-half of the values at each end of the duct section. The computation of $\alpha$, $\beta$, $\gamma$ and $\sigma$, $\tau$, $\theta$ for each section is based on the average Mach number and speed of sound in the section.

Equations (8), (10), (11) and (15) to (17) account for shock position and duct dynamics. The set provides a basic mathematical model that can be applied to a mixed-compression inlet. For the solution of a specific problem, bleeds and bypasses must be accounted for, an equation for the termination of the final subsonic section must be provided and the disturbance must be related to the system variables ($\tilde{P}$, $\tilde{W}$, and $\tilde{S}$).

## Disturbance Equations

When perturbations occur ahead of the normal shock (in the supersonic flow region), the perturbation actually represents the upstream boundary condition. This is true because the waves represented by equations (15) to (17) all travel in the downstream direction. Thus for a perturbation $\delta$ at station 0 upstream of the inlet

$$\left.\begin{aligned} \tilde{P}_0 &= q_1 \delta \\ \tilde{W}_0 &= q_2 \delta \\ \tilde{S}_0 &= q_3 \delta \end{aligned}\right\} \qquad (18)$$

where the q's represent constant coefficients. A pure flow perturbation, for example, would have $q_1 = 0$, $q_2 = 1$, and $q_3 = 0$.

## Exit Boundary Condition

As in reference 9 it is assumed that the airflow at the inlet exit is choked. With the additional assumptions that the specific heat ratio is constant and equal to 1.4, the equation for the exit boundary condition is (ref. 9):

$$\frac{\Delta \dot{W}_E}{\overline{\dot{W}}_E} = \frac{\Delta A_E}{\overline{A}_E} + \frac{6}{7}\frac{\Delta P_{T,E}}{\overline{P}_{T,E}} - \frac{1}{7}\frac{\Delta S_E}{R} \tag{19}$$

If the inlet has bleed or bypass flows, the steady-state exit flow $\overline{\dot{W}}_E$ will not be equal to the inlet flow $\overline{\dot{W}}_\infty$. Since all flows are normalized to $\overline{\dot{W}}_\infty$, equation (19) must be multiplied by the ratio $\overline{\dot{W}}_E/\overline{\dot{W}}_\infty$. Therefore,

$$\frac{\Delta \dot{W}_E}{\overline{\dot{W}}_\infty} = \frac{\overline{\dot{W}}_E}{\overline{\dot{W}}_\infty}\left(\frac{\Delta A_E}{\overline{A}_E} + \frac{6}{7}\frac{\Delta P_{T,E}}{\overline{P}_{T,E}} - \frac{1}{7}\frac{\Delta S_E}{R}\right) \tag{20}$$

Assuming that the exit area is constant $(\Delta A_E = 0)$ and taking the Laplace transform, equation (20) becomes

$$\tilde{\dot{W}}_E = \frac{6}{7}\frac{\overline{\dot{W}}_E}{\overline{\dot{W}}_\infty}\tilde{P}_E - \frac{1}{7}\frac{\overline{\dot{W}}_E}{\overline{\dot{W}}_\infty}\tilde{S}_E \tag{21}$$

It should be noted that any boundary condition that can be described in terms of the system variables ($\tilde{P}$, $\tilde{\dot{W}}$, $\tilde{S}$) could be used.

## Bleed and Bypass Airflow Equation

Supersonic inlets often have bleed and bypass airflows for such things as boundary-layer control and matching inlet airflow to engine airflow requirements. These airflows (hereinafter called bypass flow) should be accounted for because they affect the gains of normal shock position and inlet pressures to the perturbation variable. Equations for these airflows will now be derived based on choked flow conditions in order to be consistent with the experimental inlet that will be discussed later. A typical bypass flow in the wall of an inlet duct is shown in figure 2. It is assumed that the bypass flow occurs over a zero length section of duct and that the bypass area is constant.

Since the bypass is choked, the form of equation (21) applies such that

$$\tilde{\dot{W}}_{by} = \frac{6}{7}\frac{\overline{\dot{W}}_{by}}{\overline{\dot{W}}_\infty}\tilde{P}_{by} - \frac{1}{7}\frac{\overline{\dot{W}}_{by}}{\overline{\dot{W}}_\infty}\tilde{S}_{by} \tag{22}$$

Since the bypass is in the side of the duct, it is assumed that the total pressure acting on the bypass is equal to the static pressure at station n. Hence, $P_{by} = p_n$ where $\tilde{p} = (\Delta P_s(s)/\overline{P}_s)$ and in addition $\tilde{S}_{by} = \tilde{S}_n$. Reference 9 showed that

$$\tilde{p}_n = c_{Pn}\tilde{P}_n + c_{Wn}\tilde{\dot{W}}_n + c_{Sn}\tilde{S}_n \tag{23}$$

where

$$c_{Pn} = \frac{\overline{M}_n^2 + 5}{5\left(1 - \overline{M}_n^2\right)}$$

$$c_{Wn} = -\frac{7\overline{M}_n^2}{5\left(1 - \overline{M}_n^2\right)}$$

$$c_{Sn} = -\frac{\overline{M}_n^2}{5\left(1 - \overline{M}_n^2\right)}$$

Therefore, in terms of variables at station n, equation (22) becomes

$$\tilde{\dot{W}}_{by} = \frac{6}{7}\frac{\overline{\dot{W}}_{by}}{\overline{\dot{W}}_\infty} c_{Pn}\tilde{P}_n + \frac{6}{7}\frac{\overline{\dot{W}}_{by}}{\overline{\dot{W}}_\infty} c_{Wn}\tilde{\dot{W}}_n + \frac{1}{7}\frac{\overline{\dot{W}}_{by}}{\overline{\dot{W}}_\infty}\left(6c_{Sn} - 1\right)\tilde{S}_n \tag{24}$$

## MATRIX SOLUTION OF EQUATIONS

Even though time domain solutions of the complete set of equations is difficult because of the algebraic complexity, a closed-form matrix solution for the shock position transfer function can be obtained. In matrix form the normal shock equations (8), (10) and (11) become

$$\begin{bmatrix} \tilde{P}_2 \\ \tilde{\dot{W}}_2 \\ \tilde{S}_2 \end{bmatrix} = \begin{bmatrix} C_4 & \frac{C_1}{C_r} & \frac{C_1}{7} \\ 0 & 1 & 0 \\ \frac{6}{7}C_1 & -\frac{C_1}{C_r} & C_5 \end{bmatrix} \begin{bmatrix} \tilde{P}_1 \\ \tilde{\dot{W}}_1 \\ \tilde{S}_1 \end{bmatrix} + \begin{bmatrix} -C_1\left(R_c\frac{A'}{A} + C_2 s\right) \\ \left(C_B + C_r C_3 s\right) \\ C_1\left(R_c\frac{A'}{A} - C_3 s\right) \end{bmatrix} \tilde{X}_s$$

or to use a short notation form

$$T_2 = HT_1 + G\tilde{X}_s \tag{25}$$

In general, to relate conditions at two stations $n$ and $n + 1$, the wave equations (15) to (17) are used. In matrix form they become

$$\begin{bmatrix} 1 & \alpha & \beta \\ 1 & -\alpha & -\gamma \\ 0 & 0 & 1 \end{bmatrix} \begin{bmatrix} \tilde{P}_{n+1} \\ \tilde{W}_{n+1} \\ \tilde{S}_{n+1} \end{bmatrix} = \begin{bmatrix} e^{-\sigma s} & 0 & 0 \\ 0 & e^{\tau s} & 0 \\ 0 & 0 & e^{-\theta s} \end{bmatrix} \begin{bmatrix} 1 & \alpha & \beta \\ 1 & -\alpha & -\gamma \\ 0 & 0 & 1 \end{bmatrix} \begin{bmatrix} \tilde{P}_n \\ \tilde{W}_n \\ \tilde{S}_n \end{bmatrix} \tag{26}$$

or

$$BT_{n+1} = DBT_n$$

and

$$T_{n+1} = B^{-1} DBT_n = ET_n \tag{27}$$

(where $B^{-1}$ is the inverse matrix of B).

It was shown in reference 9 that the elements of E, $\epsilon_{ij}$ are

$$\epsilon_{11} = \frac{\left(e^{-\sigma s} + e^{\tau s}\right)}{2}$$

$$\epsilon_{12} = \frac{\alpha\left(e^{-\sigma s} - e^{\tau s}\right)}{2}$$

$$\epsilon_{13} = \frac{\beta\left(e^{-\sigma s} - e^{-\theta s}\right)}{2} - \frac{\gamma\left(e^{\tau s} - e^{-\theta s}\right)}{2}$$

$$\epsilon_{21} = \frac{\epsilon_{12}}{\alpha^2}$$

$$\epsilon_{22} = \epsilon_{11}$$

$$\epsilon_{23} = \frac{\beta\left(e^{-\sigma s} - e^{-\theta s}\right)}{2\alpha} + \frac{\gamma\left(e^{\tau s} - e^{-\theta s}\right)}{2\alpha}$$

$$\epsilon_{31} = \epsilon_{32} = 0$$

$$\epsilon_{33} = e^{-\theta s}$$

The equations relating variables across a choked bleed or bypass are

$$\tilde{P}_{n+1} = \tilde{P}_n$$

$$\tilde{\dot{W}}_{n+1} = \tilde{\dot{W}}_n - \tilde{\dot{W}}_{by}$$

$$\tilde{S}_{n+1} = \tilde{S}_n$$

Using equation (24) for $\tilde{\dot{W}}_{by}$, the matrix form of these equations becomes

$$\begin{bmatrix} \tilde{P}_{n+1} \\ \tilde{\dot{W}}_{n+1} \\ \tilde{S}_{n+1} \end{bmatrix} = \begin{bmatrix} 1 & 0 & 0 \\ -\frac{6}{7}\frac{\overline{\dot{W}}_{by}}{\overline{\dot{W}}_\infty} c_{Pn} & 1 - \frac{6}{7}\frac{\overline{\dot{W}}_{by}}{\overline{\dot{W}}_\infty} c_{Wn} & -\frac{1}{7}\frac{\overline{\dot{W}}_{by}}{\overline{\dot{W}}_\infty}\left(6c_{Sn} - 1\right) \\ 0 & 0 & 1 \end{bmatrix} \begin{bmatrix} \tilde{P}_n \\ \tilde{\dot{W}}_n \\ \tilde{S}_n \end{bmatrix} \tag{28}$$

or

$$T_{n+1} = E_{by} T_n \tag{29}$$

Equation (21) for the exit boundary condition in matrix form is

$$\begin{bmatrix} \overline{\dot{W}}_E / \overline{\dot{W}}_\infty \\ -7/6 \\ -\overline{\dot{W}}_E / 6\overline{\dot{W}}_\infty \end{bmatrix}^T \begin{bmatrix} \tilde{P}_E \\ \tilde{\dot{W}}_E \\ \tilde{S}_E \end{bmatrix} = 0$$

or

$$F^{T}T_{E} = 0 \tag{30}$$

All that remains is to write a matrix equation relating the perturbation and the inlet variables. In matrix form the expressions describing the perturbation (upstream boundary condition), equations (18) become

$$\begin{bmatrix} \tilde{P}_0 \\ \tilde{W}_0 \\ \tilde{S}_0 \end{bmatrix} = \begin{bmatrix} q_1 \\ q_2 \\ q_3 \end{bmatrix} \delta$$

or

$$T_0 = Q\delta \tag{31}$$

The equations ((25), (27), and (29) to (31)) can then be used to form a matrix solution for determining the transfer function between shock position and the perturbation. To demonstrate the matrix solution, an example will now be presented.

Consider a case in which a perturbation in total pressure occurs at the inlet spike-tip station. The inlet for the example is shown schematically in figure 3. To simplify the example, only four sections were used, but more sections could be used to better approximate the variation in duct area. The analysis begins with equation (25)

$$T_2 = HT_1 + G\tilde{X}_s \tag{25}$$

Variables at station 1 can be related to those at the cowl-lip station, 0', by using equation (27)

$$T_1 = E_b T_{0'}$$

and

$$T_{0'} = E_a T_0$$

or

$$T_1 = E_b E_a T_0$$

Substituting for $T_1$, equation (25) becomes

$$T_2 = HE_b E_a T_0 + G\tilde{X}_s \tag{32}$$

Equation (31) relates $T_0$ to the disturbance and is repeated here:

$$T_0 = Q\delta \tag{31}$$

where, for this example,

$$Q = \begin{bmatrix} 1 \\ 0 \\ 0 \end{bmatrix} \quad \text{and} \quad \delta = \tilde{P}_0$$

since $P_{T,0}$ is the only variable perturbed. Using (31), equation (32) becomes

$$T_2 = HE_b E_a Q\tilde{P}_0 + G\tilde{X}_s \tag{33}$$

Using equations (27), (29), and (30) results in

$$T_3 = E_c T_2$$

$$T_4 = E_{by} T_3$$

$$T_E = E_d T_4$$

$$F^T T_E = 0$$

and

$$F^T E_d E_{by} E_c T_2 = 0$$

Therefore, multiplying both sides of equation (33) by $F^T E_d E_{by} E_c$ yields

$$0 = F^T E_d E_{by} E_c H E_b E_a Q \tilde{P}_0 + F^T E_d E_{by} E_c G \tilde{X}_s$$

or

$$F^T E_d E_{by} E_c G \tilde{X}_s = - F^T E_d E_{by} E_c H E_b E_a Q \tilde{P}_0 \tag{34}$$

Since $F^T E_d E_{by} E_c G$ and $F^T E_d E_{by} E_c H E_b E_a Q$ are scalars, equation (34) becomes

$$\frac{\tilde{X}_s}{\tilde{P}_0} = - \frac{F^T E_d E_{by} E_c H E_b E_a Q}{F^T E_d E_{by} E_c G} \tag{35}$$

The elements of the E and G matrixes are functions of the Laplace variable s. Equation (35) thus represents the transfer function of shock position to the perturbation (in total pressure for the example). By substituting $s = j\omega$, the frequency response may be calculated by carrying out the matrix operations in complex algebra. This is done easily and quickly by a digital computer. Substitution of the shock position response into equation (33) as

$$T_2 = H E_b E_a Q \tilde{P}_0 + G \frac{\tilde{X}_s}{\tilde{P}_0} \tilde{P}_0$$

gives the response for the elements of $T_2$. Substituting these results into equation (27) gives the response for the elements of $T_3$ and so on down the duct. Thus, the frequency response of total pressure, flow rate, and entropy are obtained at all stations. The response of static pressure at any station n is obtained using equation (23), which in matrix form is

$$\begin{bmatrix} \tilde{p}_n \\ 0 \\ 0 \end{bmatrix} = \begin{bmatrix} c_{Pn} \\ c_{Wn} \\ c_{Sn} \end{bmatrix}^T \begin{bmatrix} \tilde{P}_n \\ \tilde{W}_n \\ \tilde{S}_n \end{bmatrix} \tag{36}$$

## COMPARISON OF ANALYSIS WITH METHOD OF CHARACTERISTICS

Reference 11 gives transfer functions for shock position to perturbations in variables just ahead of the shock, and frequency response results that were compared with experimental data from reference 13. A method of characteristics solution was also included

in reference 11 as a means for comparison since it is a very accurate analytical technique (although computer time consuming). To evaluate the merit of the small perturbation analysis of this report as an analytical technique, it is compared in figure 4 with method-of-characteristics results from reference 11. The perturbed variable is Mach number just ahead of the normal shock. For the small perturbation analysis this is represented as a flow perturbation with the aid of equation (59) from reference 9:

$$\frac{\Delta M}{\overline{M}} = \frac{5 + \overline{M}^2}{5\left(\overline{M}^2 - 1\right)} \left( \frac{\Delta P_T}{\overline{P}_T} + \frac{\Delta A}{\overline{A}} - \frac{\Delta \dot{W}}{\overline{\dot{W}}} - \frac{\Delta a_T}{\bar{a}_T} \right) \tag{37}$$

Assuming that area, total temperature, and pressure are held constant results in

$$\frac{\Delta \dot{W}_1}{\overline{\dot{W}}_1} = - \frac{5\left(\overline{M}_1^2 - 1\right)}{\left(5 + \overline{M}_1^2\right)\overline{M}_1} \Delta M_1$$

And in matrix form the perturbation equation (31) is

$$\begin{bmatrix} \tilde{P}_1 \\ \tilde{\dot{W}}_1 \\ \tilde{S}_1 \end{bmatrix} = \begin{bmatrix} 0 \\ - \dfrac{5\left(\overline{M}_1^2 - 1\right)}{\overline{M}_1\left(5 + \overline{M}_1^2\right)} \\ 0 \end{bmatrix} \Delta M_1$$

Table I gives the numerical values for parameters used in the small perturbation analysis. No bleeds or bypasses were included in either analysis.

The free-stream conditions were the same as the experimental test conditions (ref. 13). The station Mach numbers are the same as those that were used in the method-of-characteristics solution and were supplied directly by the author. The A'/A parameter calculation was based on the duct area distribution used in the method-of-characteristics analysis (ref. 11, fig. 28) and an assumed steady-state shock position 41 centimeters aft of the cowl-lip station.

The comparison of shock-position responses for the small perturbation and method of characteristics analyses (fig. 4) shows excellent agreement in both amplitude and phase. The results indicate that the small perturbation analysis is comparable in accuracy to the method-of-characteristics analysis for this application. In comparing the results of either analysis with experimental results it should be remembered that neither technique includes viscous effects and that the problem is really three dimensional.

Thus, the choice of coefficients, such as $A'/A$ and $C_B$ in the small perturbation analysis, will have considerable effect on the accuracy of the results.

## COMPARISON OF ANALYTICAL RESULTS WITH EXPERIMENTAL DATA

Frequency response tests were conducted on a mixed-compression inlet in the Lewis 10- by 10-foot supersonic wind tunnel. Perturbations both upstream and downstream of the normal shock were investigated and the results are reported in reference 13. As a means of verifying the analysis presented in this report, analytical results are compared with experimental data obtained from the upstream perturbations.

A schematic diagram of the inlet and disturbance device setup is shown in figure 5. The disturbance was produced by a gust-generator plate located above and ahead of the inlet. The plate was oscillated sinusoidally at frequencies of 1 to 15 hertz to positive and negative angles of attack. This motion produces a perturbation in the flow-field Mach number and flow-angle ahead of the inlet. (A derivation for the disturbance will be given in the next section.) A frequency response of plate angle to command voltage is shown in figure 6. It shows that the amplitude decreases with increasing frequency and at 15 hertz is only 0.36 times its low-frequency amplitude.

The inlet was sized for operation with a General Electric Company J85-13 turbojet engine and was alternately coupled to the engine or a long pipe. Provisions were made for choking the pipe airflow at either of two stations (fig. 5) and are designated as the short-pipe and long-pipe terminations. Design details of the inlet system and its steady-state performance characteristics are reported in reference 14, and a performance bleed investigation is reported in reference 15.

### Derivation of Gust Generator Airflow Perturbation

Compression and expansion waves are generated by the leading edge of the plate when it is at positive and negative angles of attack ($\pm \varphi$), respectively. If only small and slow deflections in $\varphi$ are considered, the first-order effect of $\varphi$ on the static pressure ratio $\xi$ across the wave is (ref. 16, eq. (151))

$$\xi = 1 + \frac{1.4\, M_1^2}{\left(M_1^2 - 1\right)^{1/2}} \varphi \tag{38}$$

where $\gamma = 1.4$ and $\varphi$ is in radians. In terms of $\xi$ the Mach number $M_2$ downstream of the wave is related to Mach number $M_1$ upstream of the wave by (ref. 16, eq. (157))

$$M_2^2 = \frac{M_1^2 (6\xi + 1) - 5\left(\xi^2 - 1\right)}{\xi(\xi + 6)} \tag{39}$$

Linearization of equation (39) leads to $\left(M_1 = \text{constant}, \quad \bar{\xi} = 1, \text{ and } \overline{M}_1 = \overline{M}_2 \text{ when } \overline{\varphi} = 0\right)$

$$\Delta M_2 = - \frac{\left(\overline{M}_1^2 + 5\right)}{7\overline{M}_1} \Delta\xi \tag{40}$$

From equation (38) $\Delta\xi$ is $\left(M_1 \text{ again being constant}\right)$

$$\Delta\xi = \frac{1.4\ \overline{M}_1^2}{\left(\overline{M}_1^2 - 1\right)^{1/2}} \Delta\varphi$$

so that

$$\Delta M_2 = - \frac{\left(\overline{M}_1^2 + 5\right)\overline{M}_1}{5\left(\overline{M}_1^2 - 1\right)^{1/2}} \Delta\varphi$$

and since $\overline{M}_1 = \overline{M}_2$

$$\frac{\Delta M_2}{\overline{M}_2} = - \frac{\left(\overline{M}_2^2 + 5\right)}{5\left(\overline{M}_2^2 - 1\right)^{1/2}} \Delta\varphi \tag{41}$$

The first-order change in free-stream total pressure and entropy due to a compression or expansion wave can be shown to be zero by the equations in reference 16. Therefore,

$$\frac{\Delta P_T}{\overline{P}_T} = \frac{\Delta a_T}{\bar{a}_T} = 0$$

Neglecting the change in inlet capture area due to the change in free-stream Mach number (calculated to be only about 0.4 percent per degree of plate angle for the experimental inlet), equation (37) reduces to

$$\frac{\Delta M}{\overline{M}} = - \frac{5 + \overline{M}^2}{5\left(\overline{M}^2 - 1\right)} \frac{\Delta \dot{W}}{\overline{\dot{W}}}$$

or

$$\frac{\Delta \dot{W}}{\overline{\dot{W}}} = - \frac{5\left(\overline{M}^2 - 1\right)}{5 + \overline{M}^2} \frac{\Delta M}{\overline{M}} \tag{42}$$

Related to the plate angle perturbation the flow perturbation is (combining (41) and (42))

$$\frac{\Delta \dot{W}}{\overline{\dot{W}}} = \left(\overline{M}^2 - 1\right)^{1/2} \Delta\varphi$$

And equation (31), relating the free-stream variables to the plate angle perturbation, is

$$\begin{bmatrix} \tilde{P} \\ \tilde{\dot{W}} \\ \tilde{S} \end{bmatrix} = \begin{bmatrix} 0 \\ \left(\overline{M}^2 - 1\right)^{1/2} \\ 0 \end{bmatrix} \Delta\varphi$$

Since the analysis is one-dimensional in nature, changes in flow angularity due to the plate angle of attack (limited to $\pm 1^{\circ}$) were neglected.

## Analytical Computation Details

A schematic of the inlet, to indicate the sectioning that was used for the analysis, is presented in figure 7. Comparisons of analytical and experimental frequency response results are shown in figures 8 to 10 with the inlet coupled to a turbojet engine, or a short-pipe or long-pipe termination. Except for the location of the choked exit station, the sectioning for each case was the same - all sections up to the exit being included. When coupled to the engine, the inlet was assumed to be choked at station 9. The short-pipe and long-pipe terminations were assumed to be choked at stations 10 and 12, respectively, which correspond to the actual choke points.

The following information regarding sectioning is common to all three cases. The disturbance was assumed to occur at the intersection of the Mach wave generated by the plate at $0^{\circ}$ angle-of-attack and the longitudinal axis of the inlet (see fig. 7). Choked bleed and bypass stations were located as shown in figure 7. The steady-state normal-shock position was assumed to be the same for all cases - the center of the throat static-pressure tap region shown in figure 4. Sections were included at the throat

exit-static pressure, static pressure before bypass cavity, and engine face static-pressure tap locations because it was desired to obtain frequency responses of those variables to the plate angle perturbation. The remaining sections were included to better approximate the variation in duct cross-sectional area.

Tables II to IV contain numerical values for parameters used in the analysis, the results of which are presented in figures 8 to 10, respectively. The free-stream conditions correspond to the tunnel free-stream test conditions given in reference 13. These free-stream conditions plus the duct geometric cross-sectional area distribution were used as the basis for calculating the Mach number at each station, neglecting boundary-layer effects. The Mach number at the spike tip station was assumed to be the same as free stream.

The value of the $A'/A$ parameter was selected to make the analysis gain of shock position to plate angle of attack the same as the gain that was estimated from experimental data. The values ranged from 0.4534 to 1.1453 per meter, depending on whether the inlet had stability bleed (reflected in the analysis by coefficient $C_B$). This range of values is approximately 3 to 7 times the value determined from the inlet geometric cross-sectional area variation at the shock operating point. Because of shock-boundary layer interaction effects, the shock gain is not uniquely dependent on the geometric value of $A'/A$.

The steady-state airflow rate ratios $\overline{\dot{W}}_1/\overline{\dot{W}}_\infty$, $\overline{\dot{W}}_{by}/\overline{\dot{W}}_\infty$, and $\overline{\dot{W}}_E/\overline{\dot{W}}_\infty$ and the stability bleed coefficient $C_B$ were calculated with the aid of data found in references 13 and 15, for the inlet-engine and inlet-long pipe cases. Unpublished NASA data were used to calculate these parameters for the inlet-short pipe case.

## DISCUSSION OF RESULTS

Figure 8 shows comparisons of analysis and experimental (ref. 13) frequency response results with the inlet coupled to the J85-13 turbojet engine.

In figures 8 to 10 two sets of analytical results are shown. The solid line results include all of the transportation times given in tables II to IV, respectively. For the dashed line results the transportation times in the seven supersonic sections were set equal to zero. This demonstrates the effect of neglecting dynamics in the supersonic portion of the inlet.

The phase data are generally in good agreement for all signals. Even without the transportation times for the supersonic sections, the maximum difference in analysis phase results is about $15^\circ$ (out of $100^\circ$) at 15 hertz.

The amplitude data are presented as normalized amplitude ratios. Both experimental and analytical amplitude ratio data for each response have been normalized by dividing by the low-frequency value of the amplitude ratio determined from experimental data. The amplitude data do not agree as well as the phase data, especially the static pressure

before bypass cavity and engine-face static-pressure responses. The analysis indicates that these two signals have low-frequency gains approximately 1.6 times larger than the experimentally measured gains. This discrepancy may be due in part to the fact that the engine-face station (compressor face) is not choked as was assumed for the analysis. The effect on analysis amplitude results is negligible when the supersonic section transportation times are eliminated.

Comparisons of analytical and experimental (previously unpublished) results for the inlet-short pipe termination case are shown in figure 9. The plots for static pressure before the bypass cavity and for static pressure at the engine face are not given because these experimental responses were not taken. For this case both amplitude and phase data are in good agreement when the transportation times for the supersonic sections are included. Without the transportation times the difference in analysis phase is as much as $25^{o}$ (out of $100^{o}$) at 15 hertz. Shock position amplitude also shows more attenuation without the transportation times.

Figure 10 shows a comparison of analytical and experimental (ref. 13) frequency response results for the inlet-long pipe combination. The plot for static pressure before the bypass cavity is not given because, again, this experimental response was not taken. As for the previous cases, the phase agreement is generally very good even with the transportation times for the supersonic sections set equal to zero. These times are less important in this case, because of the larger subsonic section transport times resulting from the longer duct. Agreement between the amplitude ratio data is good except for the throat-exit static-pressure signal. The analysis results indicate that the amplitude ratio is about 0.7 times the experimental low-frequency value. This error may be partly due to the fact that the analysis relates variables across the normal shock which ideally is a discontinuity. In nature, a normal shock may occur as a series of shocks or a shock train which could extend to the vicinity of the throat exit static pressure.

Finally, a couple of observations will be made from the controls point of view regarding the data in general. First, for each of the cases (figs. 8 to 10) the phase lag at a forward station is greater than at an aft station; or, the phase lag increases as signal distance from the perturbation location decreases. Second, comparing figures 9 and 10 shows that the phase lag for a given signal is greater when the exit station is farther from the signal (long-pipe termination). These observations can also be made for the downstream disturbance case from data in reference 13. Thus, the inlet frequency response to a flow-field perturbation upstream of the normal shock is similar to the response resulting from a perturbation at the inlet exit. The normal shock must respond to the upstream perturbation before the subsonic duct pressures to satisfy the normal shock equations (7), (9), and (10).

## CONCLUDING REMARKS

An analysis was presented for determining the dynamic response of a supersonic inlet to perturbations ahead of the normal shock. The analysis, based primarily on the linearized, one-dimensional, distributed parameter wave equation, is applicable to analysis of mixed-compression inlets. Discontinuities and losses in the supersonic duct due to oblique shock waves are neglected. The equations are suitable for implementation on an analog computer. Also, closed-form expressions for the evaluation of frequency responses were obtained using matrix operations (no inversion required). These expressions are easily programmed on a digital computer and require little computer time to solve.

The major difficulty in applying the analysis arises in choosing the correct value of the $A'/A$ parameter. Because of shock-boundary layer interaction effects, the shock response is not uniquely dependent on the geometric value of $A'/A$. In this report an effective $A'/A$ was determined empirically from the experimentally measured gain of shock position to the perturbation variable. The effective $A'/A$ values varied from 3 to 7 times the geometric value. Further work is required to determine a means for estimating an effective $A'/A$ when experimental data are unavailable. This is important because $A'/A$ is common to most inlet analyses.

## SUMMARY OF RESULTS

Analysis frequency response results were compared with a method-of-characteristics solution over the frequency range of 5 to 40 hertz. The perturbed variable was Mach number just ahead of the normal shock. Agreement was excellent in both amplitude ratio and phase angle over the entire frequency range. The analysis has the advantages of being simpler to program and requiring much less computer time to solve.

Frequency response comparisons were also made of the analysis with experimental inlet data obtained in a wind tunnel. The perturbation frequency range was 1 to 15 hertz. Data were obtained with the inlet coupled to a turbojet engine, a short pipe, or a long pipe (the pipes having choked exit airflows). In these cases the perturbed variable was Mach number just ahead of the inlet.

Phase angle agreement was generally very good for both shock position and static pressures in the subsonic duct. When the transportation times for the supersonic duct were eliminated, the error in phase angle generally remained small except for the shock position responses with the inlet coupled to the engine or short pipe.

The $A'/A$ parameter (the rate of change of duct area with shock position divided by the duct area - evaluated at the shock operating point) was selected to assure good amplitude ratio agreement for the shock position responses. In general, the comparisons showed good agreement between the shapes of the static-pressure amplitude ratio

response curves. However, in some cases a substantial shift in gain was observed. For the inlet-engine case the analysis predicted that static pressures near the subsonic diffuser exit had a low-frequency gain 1.6 times larger than the experimental values. The discrepancy may be due in part to the fact that the engine face is not choked as was assumed for the analysis. A static pressure near the normal shock was in error by as much as 27 percent. This error is believed to be due to the fact that the analysis relates variables across the normal shock which ideally is a discontinuity. In reality this shock may occur as a series of shocks or a shock train.

Lewis Research Center,
National Aeronautics and Space Administration,
Cleveland, Ohio, September 9, 1974,
501-24.

## APPENDIX - SYMBOLS

| | |
|---|---|
| $A$ | duct cross-sectional area, $m^2$ |
| $A'$ | rate of change of duct cross-sectional area along duct, $m^2/m$ |
| $a$ | speed of sound, m/sec |
| $B$ | coefficient matrix (3 by 3) |
| $C_B$ | stability bleed coefficient, dimensionless |
| $C_r$ | ratio of airflow rates at station 1 to most upstream station, dimensionless |
| $C_1, C_4, C_5$ | coefficients, dimensionless |
| $C_2, C_3$ | coefficients, sec |
| $c_{Pn}, c_{Sn}, c_{Wn}$ | coefficients at station n, dimensionless |
| $D$ | delay matrix (3 by 3) |
| $E$ | coefficient matrix (3 by 3) |
| $F$ | coefficient vector |
| $G$ | shock position transfer function vector |
| $H$ | coefficient matrix (3 by 3) |
| $j$ | $\sqrt{-1}$ |
| $L$ | length, m |
| $M$ | Mach number, dimensionless |
| $P$ | pressure, $N/m^2$ |
| $\tilde{p}$ | Laplace transform of static pressure perturbation variable (see eq. (23)) |
| $Q$ | coefficient vector |
| $q$ | elements of Q vector |
| $R$ | universal gas constant, J/mole-K |
| $R_c$ | radius of inlet cowl measured at cowl-lip station, m |
| $S$ | entropy, J/mole-K |
| $s$ | Laplace variable, $sec^{-1}$ |
| $T$ | state vector |
| $t$ | time, sec |
| $v$ | velocity, m/sec |

| | |
|---|---|
| $\dot{W}$ | airflow rate, kg/sec |
| $X_s$ | shock position, m |
| x | space coordinate, m |
| $\alpha, \beta, \gamma$ | wave equation coefficients, dimensionless |
| $\Delta$ | perturbation quantity |
| $\delta$ | perturbation variable in Laplace domain |
| $\epsilon$ | elements of E matrix |
| $\theta, \sigma, \tau$ | transportation times, sec |
| $\xi$ | static pressure ratio across normal shock, dimensionless |
| $\varphi$ | gust-generator plate angle of attack, rad or deg |
| $\omega$ | frequency, rad/sec |

Subscripts:

| | |
|---|---|
| a, b, c, d | duct section identification for example problem |
| av | average value (one-half the sum of values at each end of duct section) |
| B | stability bleed |
| by | choked bypass or bleed |
| E | exit conditions |
| ij | $i^{th}$ row, $j^{th}$ column location of matrix element |
| n | station or section number associated with variable |
| s | static condition |
| T | total or stagnation condition |
| 0, 0' | stations upstream of normal shock for example problem |
| 1 | station number just ahead of normal shock |
| 2 | station number just aft of normal shock |
| 3, 4 | stations downstream of normal shock for example problem |
| $\infty$ | most upstream station |

Superscripts:

| | |
|---|---|
| $\bar{}$ | steady-state value of variable |
| $\sim$ | Laplace transform of nondimensional small perturbation variable |
| T | transpose of matrix |

## REFERENCES


1. Neiner, George H.; Crosby, Michael J.; and Cole, Gary L.: Experimental and Analytical Investigation of Fast Normal Shock Position Controls for a Mach 2.5 Mixed-Compression Inlet. NASA TN D-6382, 1971.

2. Cole, Gary L.; Neiner, George H.; and Baumbick, Robert J.: Terminal Shock Position and Restart Control of a Mach 2.7 Two-Dimensional, Twin-Duct, Mixed-Compression Inlet. NASA TM X-2818, 1973.

3. Cole, Gary L.; Neiner, George H.; and Wallhagen, Robert E.: Coupled Supersonic Inlet-Engine Control Using Overboard Bypass Doors and Engine Speed to Control Shock Position. NASA TN D-6019, 1970.

4. Neiner, George H.; Cole, Gary L.; and Arpasi, Dale J.: Digital-Computer Normal-Shock-Position and Restart Control of a Mach 2.5 Axisymmetric Mixed-Compression Inlet. NASA TN D-6880, 1972.

5. Chun, K. S.; and Burr, R. H.: A Control System Concept for an Axisymmetric Supersonic Inlet. J. Aircraft, vol. 6, no. 4, July-Aug. 1969, pp. 306-311.

6. Sanders, John C.: Control of Supersonic Propulsion Systems. Paper presented at Sixth Anglo-American Aeronautical Conference, Folkestone, September, 9-12, 1957.

7. Himmel, Seymour C.: Application of the Method of Coordinate Perturbation to Unsteady Duct Flow. NACA TM-1439, 1958.

8. Hurrell, Herbert G.: Analysis of Shock Motion in Ducts During Disturbances in Downstream Pressure. NACA TN-4090, 1957.

9. Willoh, Ross G.: A Mathematical Analysis of Supersonic Inlet Dynamics. NASA TN D-4969, 1968.

10. Martin, Arnold W.: Propulsion System Dynamic Simulation Theory and Equations. NASA CR-928, 1968.

11. Barry, Frank W.: Frequency of Supersonic Inlet Unstarts Due to Atmospheric Turbulence. HSER-5838, Hamilton Standard (NASA CR-137482), 1973.

12. Wasserbauer, Joseph F.; and Willoh, Ross G.: Experimental and Analytical Investigation of the Dynamic Response of a Supersonic Mixed-Compression Inlet. Paper 68-651, AIAA, June 1968.

13. Wasserbauer, Joseph F.: Dynamic Response of a Mach 2.5 Axisymmetric Inlet with Engine or Cold Pipe and Utilizing 60 Percent Supersonic Internal Area Contraction. NASA TN D-5338, 1969.

14. Cubbison, Robert W., Meleason, Edward T.; and Johnson, David F.: Performance Characteristics from Mach 2.58 tc 1.98 of an Axisymmetric Mixed-Compression Inlet System with 60-Percent Internal Contraction. NASA TM X-1739, 1969.

15. Cubbison, Robert W.; Meleason, Edward T.; and Johnson, David F.: Effect of Porous Bleed in a High-Performance Axisymmetric, Mixed-Compression Inlet at Mach 2.5. NASA TM X-1692, 1968.

16. Equations, Tables, and Charts for Compressible Flow. NACA TR-1135, 1953.

TABLE I.- NUMERICAL VALUES FOR PARAMETERS USED IN ANALYSIS COMPARISON WITH METHOD-OF-CHARACTERISTICS SOLUTION[a]

[Free-stream test conditions: total pressure, 10.05 $N/cm^2$; total temperature, 342 K; Mach number, 2.497; area ratio parameter, $A'/A$, 0.961 $m^{-1}$.]

| Station | Distance from cowl-lip, cm | Mach number | Section between stations | Transportation time, msec | | |
|---|---|---|---|---|---|---|
| | | | | $\sigma$ | $\tau$ | $\theta$ |
| 1 | 41 | 1.3 | ------ | ---- | ---- | ---- |
| 2 | 41 | .786 | 1 to 2 | ---- | ---- | ---- |
| 3 | 47 | .684 | 2 to 3 | 0.098 | 0.642 | 0.232 |
| 4 | 54 | .651 | 3 to 4 | .118 | .592 | .295 |
| 5 | 60 | .592 | 4 to 5 | .104 | .444 | .270 |
| 6 | 70 | .479 | 5 to 6 | .181 | .597 | .519 |
| 7 | 80 | .427 | 6 to 7 | .189 | .503 | .608 |
| 8 | 90 | .391 | 7 to 8 | .195 | .464 | .670 |
| 9 | 100 | .363 | 8 to 9 | .199 | .439 | .725 |
| 10 | 110 | .369 | 9 to 10 | .200 | .431 | .747 |
| 11 | 120 | .381 | 10 to 11 | .199 | .437 | .730 |
| 12 | 130 | .369 | 11 to 12 | .199 | .437 | .730 |
| 13 | 140 | .358 | 12 to 13 | .200 | .429 | .752 |

[a]See fig. 4.

TABLE II. - NUMERICAL VALUES FOR PARAMETERS USED IN INLET WITH ENGINE ANALYSIS[a]

[Free-stream test conditions: total pressure, 9.98 $N/cm^2$; total temperature, 342.0 K; Mach number, 2.498. Stability bleed coefficient, 0; area ratio parameter, A'/A, 0.4534 $m^{-1}$. Steady-state airflow rate ratios: $\dot{W}_{by}/\dot{W}_{\infty}$ at station 5', 0.015; $\dot{W}_{by}/\dot{W}_{\infty}$ at station 3', 0.025; $\dot{W}_{by}/\dot{W}_{\infty}$ at station 6, 0.116; $\dot{W}_1/\dot{W}_{\infty}$, 0.958; $\dot{W}_E/\dot{W}_{\infty}$ at station 9, 0.842.]

| Station | Mach number | Section between stations | Transportation time, msec | | |
|---|---|---|---|---|---|
| | | | $\sigma$ | $\tau$ | $\theta$ |
| 8' | 2.498 | ------ | ---- | ----- | ---- |
| 7' | 2.498 | 8' to 7' | 0.793 | -1.851 | 1.110 |
| 6' | 2.252 | 7' to 6' | .554 | -1.363 | .788 |
| 5' | 1.513 | 6' to 5' | .359 | -1.201 | .553 |
| 4' | 1.539 | 5' to 4' | 0 | 0 | 0 |
| 3' | 1.383 | 4' to 3' | .046 | - .248 | .078 |
| 2' | 1.434 | 3' to 2' | 0 | 0 | 0 |
| 1 | 1.390 | 2' to 1 | .116 | - .677 | .198 |
| 2 | .744 | 1 to 2 | 0 | 0 | 0 |
| 3 | .722 | 2 to 3 | .094 | .605 | .221 |
| 4 | .640 | 3 to 4 | .139 | .729 | .342 |
| 5 | .388 | 4 to 5 | .676 | 2.096 | 1.998 |
| 6 | .377 | 5 to 6 | .305 | .682 | 1.102 |
| 7 | .324 | 6 to 7 | 0 | 0 | 0 |
| 8 | .335 | 7 to 8 | .456 | .905 | 1.842 |
| 9 | .322 | 8 to 9 | .106 | .210 | .430 |

[a]See fig. 8.

TABLE III. - NUMERICAL VALUES FOR PARAMETERS USED IN INLET WITH SHORT-PIPE-ANALYSIS[a]

[Free-stream test conditions: total pressure, 8.94 $N/cm^2$; total temperature 313.4 K; Mach number, 2.498. Stability bleed coefficient, 0.037; area ratio parameter, A'/A, 1.1453 $m^{-1}$. Steady-state airflow rate ratios: $\overline{W}_{by}/\overline{W}_{\infty}$ at station 5', 0.015; $\overline{W}_{by}/\overline{W}_{\infty}$ at station 3', 0.025; $\overline{W}_{by}/\overline{W}_{\infty}$ at station 6, 0.135; $\overline{W}_1/\overline{W}_{\infty}$, 0.958; $\overline{W}_E/\overline{W}_{\infty}$ at station 10, 0.806.]

| Station | Mach number | Section between stations | Transportation time, msec | | |
|---|---|---|---|---|---|
| | | | $\sigma$ | $\tau$ | $\theta$ |
| 8' | 2.498 | ------- | ----- | ----- | ----- |
| 7' | 2.498 | 8' to 7' | 0.828 | -1.934 | 1.160 |
| 6' | 2.252 | 7' to 6' | .579 | -1.424 | .823 |
| 5' | 1.514 | 6' to 5' | .375 | -1.255 | .578 |
| 4' | 1.539 | 5' to 4' | 0 | 0 | 0 |
| 3' | 1.383 | 4' to 3' | .048 | - .259 | .081 |
| 2' | 1.435 | 3' to 2' | 0 | 0 | 0 |
| 1 | 1.407 | 2' to 1 | .121 | - .694 | .205 |
| 2 | .737 | 1 to 2 | 0 | 0 | 0 |
| 3 | .698 | 2 to 3 | .098 | .597 | .235 |
| 4 | .621 | 3 to 4 | .146 | .713 | .368 |
| 5 | .377 | 4 to 5 | .712 | 2.123 | 2.145 |
| 6 | .365 | 5 to 6 | .321 | .699 | 1.185 |
| 7 | .305 | 6 to 7 | 0 | 0 | 0 |
| 8 | .313 | 7 to 8 | .483 | .917 | 2.045 |
| 9 | .301 | 8 to 9 | .113 | .213 | .479 |
| 10 | .345 | 9 to 10 | .362 | .708 | 1.482 |

[a]See fig. 9.

TABLE IV. - NUMERICAL VALUES FOR PARAMETERS USED IN INLET WITH LONG-PIPE-ANALYSIS[a]

[Free-stream test conditions: total pressure, 9.02 $N/cm^2$; total temperature, 316.0 K; Mach number, 2.498. Stability bleed coefficient, 0; area ratio parameter, A'/A, 0.4716 $m^{-1}$. Steady-state airflow rate ratios: $\dot{W}_{by}/\dot{W}_{\infty}$ at station 5', 0.015; $\dot{W}_{by}/\dot{W}_{\infty}$ at station 3', 0.025; $\dot{W}_{by}/\dot{W}_{\infty}$ at station 6, 0.098; $\dot{W}_1/\dot{W}_{\infty}$, 0.958; $\dot{W}_E/\dot{W}_{\infty}$ at station 12, 0.860.]

| Station | Mach number | Section between stations | Transportation time, msec | | |
|---|---|---|---|---|---|
| | | | $\sigma$ | $\tau$ | $\theta$ |
| 8' | 2.498 | ------- | ----- | ----- | ----- |
| 7' | 2.498 | 8' to 7' | 0.825 | -1.926 | 1.155 |
| 6' | 2.252 | 7' to 6' | .577 | -1.418 | .820 |
| 5' | 1.513 | 6' to 5' | .374 | -1.250 | .575 |
| 4' | 1.538 | 5' to 4' | 0 | 0 | 0 |
| 3' | 1.382 | 4' to 3' | .048 | - .258 | .081 |
| 2' | 1.434 | 3' to 2' | 0 | 0 | 0 |
| 1 | 1.390 | 2' to 1 | .120 | - .705 | .206 |
| 2 | .744 | 1 to 2 | 0 | 0 | 0 |
| 3 | .718 | 2 to 3 | .097 | .626 | .230 |
| 4 | .634 | 3 to 4 | .144 | .747 | .358 |
| 5 | .379 | 4 to 5 | .707 | 2.147 | 2.107 |
| 6 | .366 | 5 to 6 | .319 | .698 | 1.176 |
| 7 | .323 | 6 to 7 | 0 | 0 | 0 |
| 8 | .330 | 7 to 8 | .476 | .937 | 1.934 |
| 9 | .316 | 8 to 9 | .111 | .217 | .455 |
| 10 | .362 | 9 to 10 | .357 | .723 | 1.408 |
| 11 | .330 | 10 to 11 | .604 | 1.243 | 2.348 |
| 12 | .342 | 11 to 12 | 4.161 | 8.375 | 16.536 |

[a]See fig. 10.

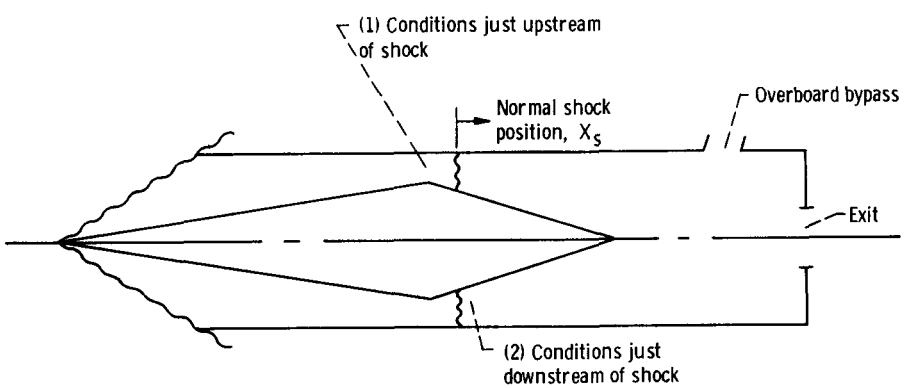


Figure 1. - Idealized mixed-compression inlet.

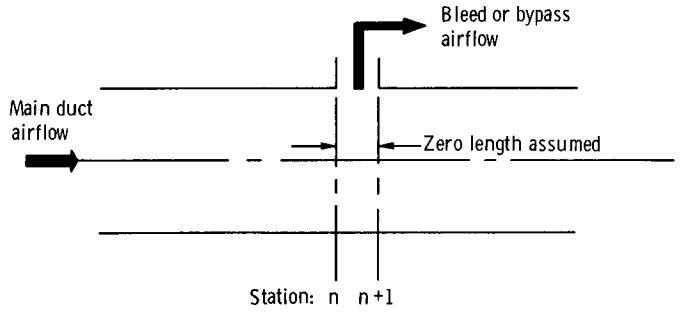


Figure 2. - Bleed or bypass airflow in inlet duct.

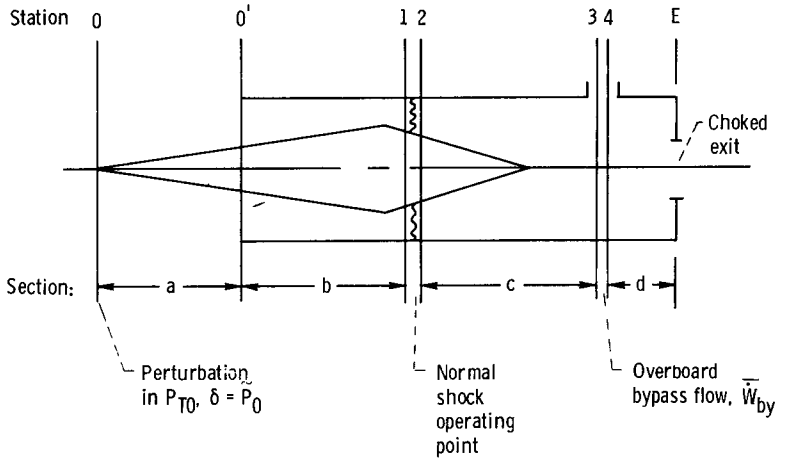


Figure 3. - Schematic of inlet for example problem.

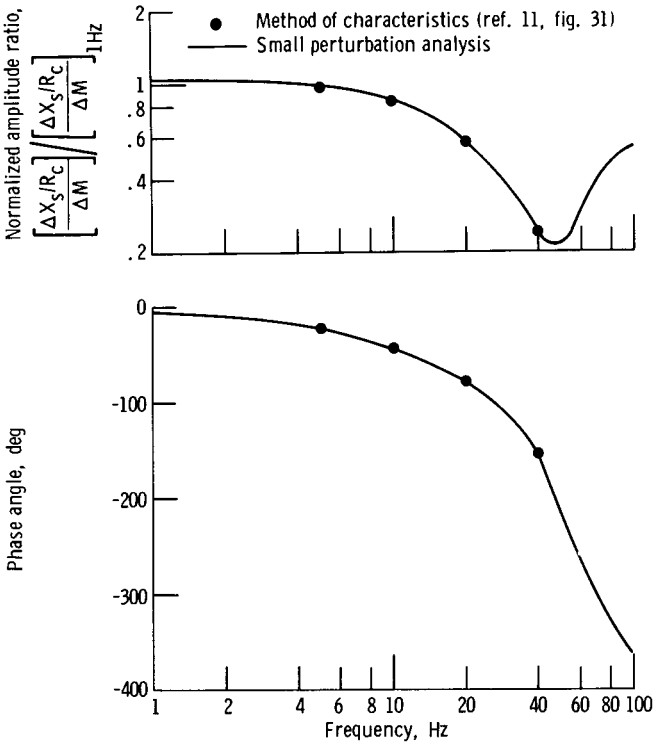


Figure 4. - Comparison of small perturbation analysis with method-of-characteristics solution. Response of shock position to perturbation in Mach number just upstream of shock. Normalizing amplitude ratio, 2.067. (Numerical values of parameters used in analysis given in table I.)

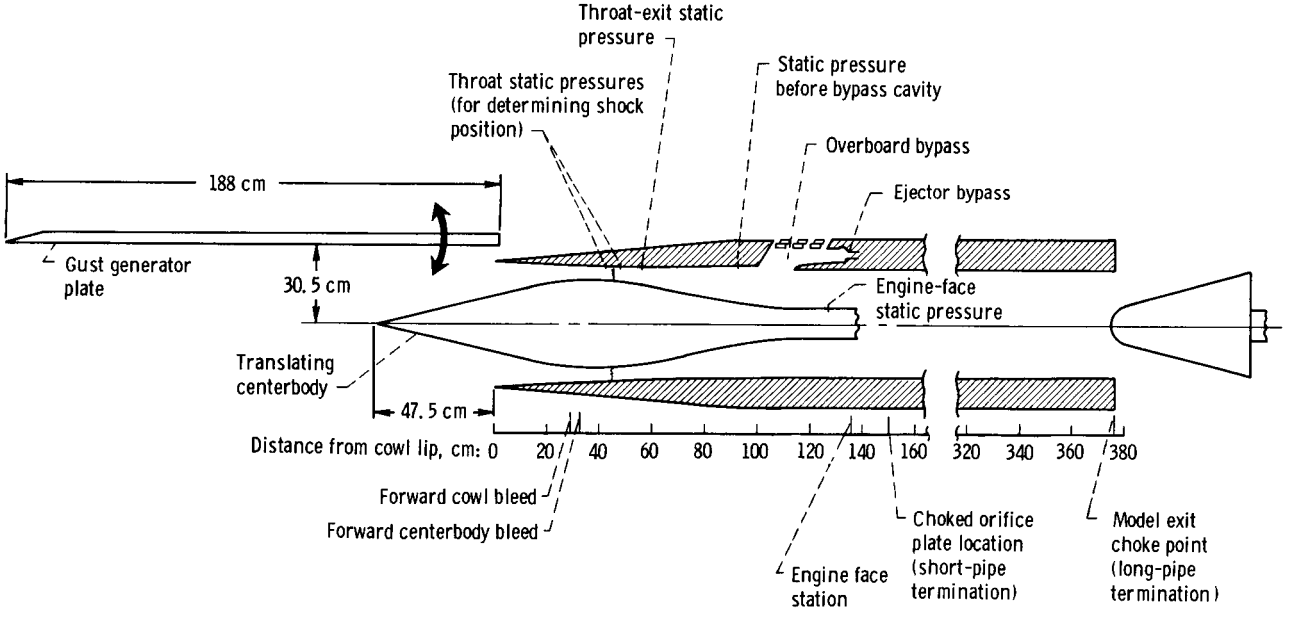


Figure 5. - Schematic diagram of experimental mixed-compression inlet setup.

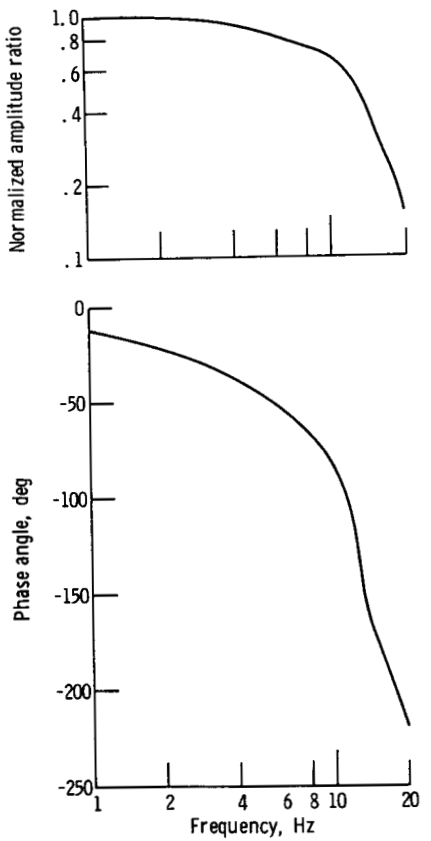


Figure 6. - Frequency response of gust-generator plate angle to command voltage (1-Hz peak-to-peak amplitude, $2^{0}$).

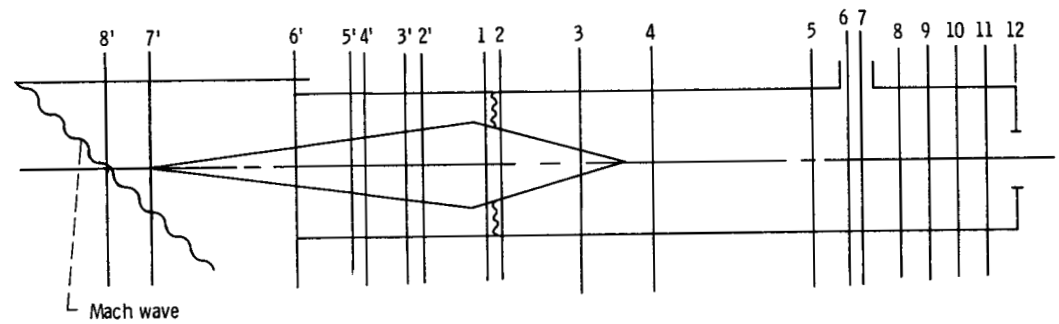


| Station number | Description | Distance from cowl lip, cm |
|---|---|---|
| 8' | Assumed gust-generator disturbance location | -116.1 |
| 7' | Centerbody tip | -47.5 |
| 6' | Cowl-lip | 0 |
| 5', 4' | Forward cowl bleed | 29.1 |
| 3', 2' | Forward centerbody bleed | 32.6 |
| 1 | Just upstream of normal shock | 41.4 |
| 2 | Just downstream of normal shock | 41.4 |
| 3 | Intermediate subsonic diffuser | 47.1 |
| 4 | Throat-exit static pressure | 55.4 |
| 5 | Static pressure before bypass cavity | 92.3 |
| 6, 7 | Center of overboard bypass opening | 107.6 |
| 8 | Engine-face static pressure | 129.9 |
| 9 | Engine face | 135.1 |
| 10 | Choked orifice plate (short-pipe termination) | 151.9 |
| 11 | Intermediate long-pipe station | 180.5 |
| 12 | Model exit choke point (long-pipe termination) | 376.4 |

Figure 7. - Schematic diagram showing inlet station locations for simulation of experimental inlet.

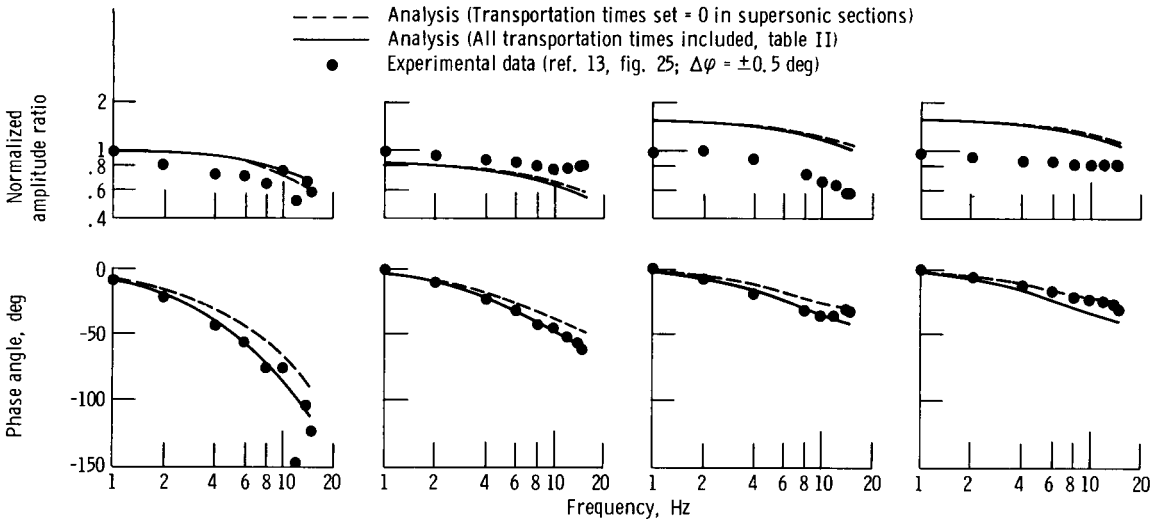


(a) Signal, shock position; normalizing amplitude ratio, $(\Delta X_s/R_c)/\Delta\varphi$, 0.3381 $deg^{-1}$.

(b) Signal, throat-exit static pressure; normalizing amplitude ratio, $(\Delta P/\bar{P})/\Delta\varphi$, 0.0464 $deg^{-1}$.

(c) Signal, static pressure before bypass cavity; normalizing amplitude ratio, $(\Delta P/\bar{P})/\Delta\varphi$, 0.0245 $deg^{-1}$.

(d) Signal, engine face static pressure; normalizing amplitude ratio, $(\Delta P/\bar{P})/\Delta\varphi$, 0.0239 $deg^{-1}$.

Figure 8. - Comparison of analysis with experimental inlet-engine response to gust-generator plate. (Numerical values for parameters used in analysis given in table II.)

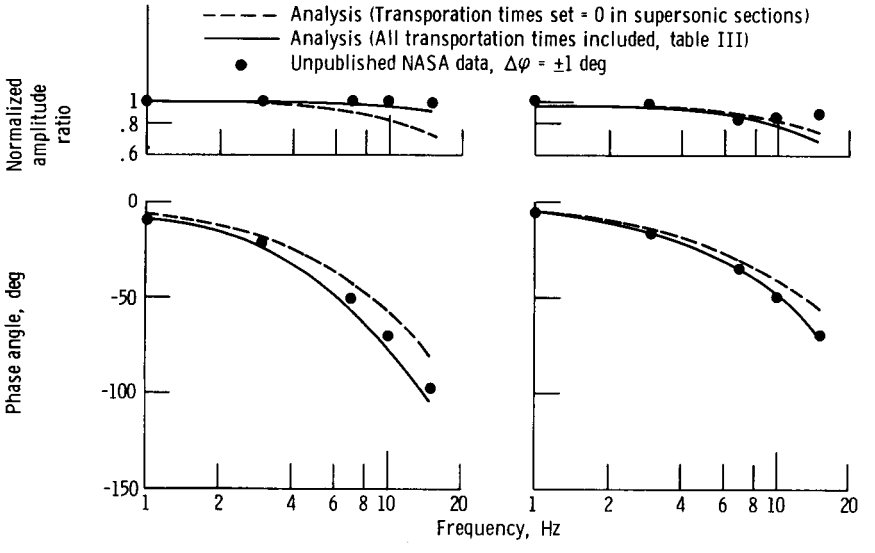


(a) Signal, shock position; normalizing amplitude ratio, $(\Delta X_s/R_c)/\Delta\varphi$, 0.1039 $deg^{-1}$.

(b) Signal, throat exit static pressure; normalizing amplitude ratio, $(\Delta P/\bar{P})/\Delta\varphi$, 0.0375 $deg^{-1}$.

Figure 9. - Comparison of analysis with experimental inlet-short-pipe response to gust-generator plate. (Numerical values for parameters used in analysis given in table III.)

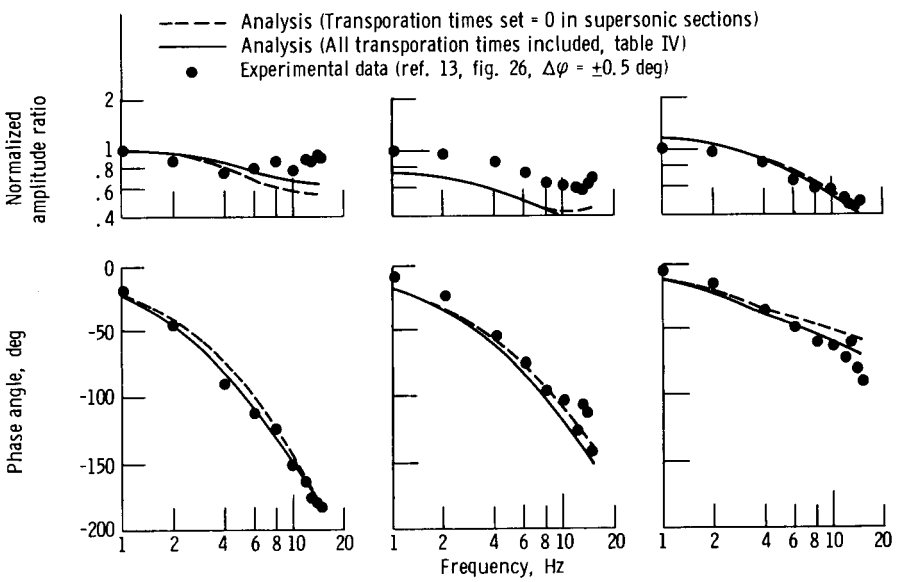


(a) Signal, shock position; normalizing amplitude ratio, $(\Delta X_s/R_c)/\Delta\varphi$, 0.3254 $deg^{-1}$.

(b) Signal, throat exit static pressure; normalizing amplitude ratio, $(\Delta P/\bar{P})/\Delta\varphi$, 0.0525 $deg^{-1}$.

(c) Signal, engine-face static pressure; normalizing amplitude ratio, $(\Delta P/\bar{P})/\Delta\varphi$, 0.0329 $deg^{-1}$.

Figure 10. - Comparison of analysis with experimental inlet-long-pipe response to gust-generator plate. (Numerical values for parameters used in analysis given in table IV.)